CrossMark

RESEARCH PAPER

Selective handling of droplets in a microfluidic device using magnetic rails

Bruno Teste · Nicolas Jamond · Davide Ferraro · Jean-Louis Viovy · Laurent Malaquin

Abstract Droplet microfluidics is currently undergoing an explosive development due to its ability to compartmentalize samples in picolitre to nanolitre volumes, transport them without dispersion and perform high-throughput analysis. The precise manipulation of single droplets, however, still requires complex chips, such as microelectrode arrays, or equipment, such as laser-based sorting. We report here a very simple proof of concept of an innovative and active technology which allows the individual manipulation of single droplets. This technology combines ferromagnetic rails and magnetic nanolitre droplets. Ferromagnetic rails are used to locally create magnetic potential wells. When the field is turned OFF, the hydrodynamic drag force transports the magnetic droplets according to the flow velocity profile. By switching ON the magnetic field, droplets experience a magnetic force that affects their trajectory when passing over the magnetized rail. The combination of the drag force exerted by the oil flow and the magnetic force resulting from the magnetized rail leads to a deflection force that guides the droplet along the rail, thus imposing a deterministic trajectory. The magnetic rails networks offer a spatially and temporally addressable guidance and sorting of individual magnetic droplets by synchronizing field activation and droplets positions. Numerical simulations were performed to evaluate spatial distribution of both drag and magnetic forces within the microdevice. The influence of different parameters such as magnetic flux density magnitude, flow rate and orientation of the rail has been investigated. Finally, selective droplet sorting, parking and merging were demonstrated and the monitoring of parallelized enzymatic reactions was performed.

Keywords Droplet microfluidics · Droplet handling · Magnetic particles · Magnetic guidance · Parallel measurements

B. Teste · N. Jamond · D. Ferraro · J.-L. Viovy · L. Malaquin (✉)
Centre de Recherche, Institut Curie, 75248 Paris, France
e-mail: laurent.malaquin@curie.fr

B. Teste
e-mail: bruno.teste@espci.fr

B. Teste · N. Jamond · D. Ferraro · J.-L. Viovy · L. Malaquin
CNRS, UMR168, 75248 Paris, France

B. Teste · N. Jamond · D. Ferraro · J.-L. Viovy · L. Malaquin
UPMC, 75248 Paris, France

B. Teste · N. Jamond · D. Ferraro · J.-L. Viovy · L. Malaquin
PSL, 75248 Paris, France

1 Introduction

Droplet microfluidics is now recognized as a major component of microfluidic systems. Microdroplets behave as miniaturized reactors with controlled content within which species or reactions can be studied or performed independently and at high throughput. Droplet microfluidics is particularly attractive for biological and chemical applications. It provides opportunities to discretize samples into small volumes, typically ranging from picolitres to nanolitres, allowing statistical studies in parallel. Droplet generation can be performed at very high rates (up to 10 kHz), thus making droplet-based platforms very well adapted for high-throughput analyses or screening (Song et al. 2006; Theberge et al. 2010). The microfluidic modules dedicated to droplets manipulation led to various chemical and

biological applications depending on the number of droplets involved in the analytical procedure. High-throughput devices were developed for studying molecules crystallization (Cohen et al. 2010) or digital PCR (Pinheiro et al. 2012). The latter, in particular, encountered a strong success, improving by two orders of magnitudes at least the sensitivity of PCR. They are ideally suited to exploit protocols playing with high statistics upon a large number of droplets following the same fate. As a drawback, though, these high-throughput generation methods can only prepare a large number of droplets from a very limited number of fluid sources (typically one or two, if coalescence is added along the production line). These platforms are thus poorly adapted to analyses involving complex analytical workflows and are mainly restricted to give droplet content at a single time point (yes/no responses). Nevertheless, these approaches encountered great successes through companies such as RainDance Technologies or Bio-Rad Laboratories. For applications in which a more moderate throughput is sufficient, but better control of each droplet composition and fate is needed, strategies involving on demand droplets generation and individual handling are preferable to control both the content and processing of droplets at the individual scale (Abbyad et al. 2011; Churski et al. 2010; Lorenz et al. 2006). The handling and identification of a smaller number of droplets give access to droplet monitoring and more accurate information.

In this context, one of the actual challenges in droplet microfluidics development relies on efficient and precise manipulation of individual droplets, to perform basic operations such as merging, splitting, sorting, trapping or guidance in both high- and low-throughput analyses. Both passive and active methods have been investigated to perform these operations. In passive approaches, droplets splitting, sorting, mixing, trapping and synchronization mainly involve topological modification of the channels including bifurcations (Adamson et al. 2006; Link et al. 2004) winding channels (Song et al. 2003) as well as the integration of 3D structures such as pillars (Niu et al. 2008; Protière et al. 2010), rail roads (Abbyad et al. 2011; Ahn et al. 2011) or chamber arrays (Huebner et al. 2009). Although passive operations are very simple to implement, most device architectures do not provide the flexibility needed for individual droplets manipulation. Passive manipulations are in general non-selective and not easily tunable. All the droplets will follow the same trajectories and operating workflow. This limitation is solved by combining passive methods with active approaches, usually based on electric, optical or magnetic principles. For instance, integrated electrodes can be used for droplets sorting (Ahn et al. 2006; Baret et al. 2009) or merging (Chabert et al. 2005; Abate et al. 2010). For example, Zagnoni and Cooper (2009) developed a system that does not require precise alignment or

droplets synchronization and where electrodes were used to slow and trap the droplets in order to force them to merge. Electrostatic forces were also successfully used to perform various operations such as droplets sorting, guidance, trapping and splitting (DeRuiter et al. 2014). The authors have shown that metallic electrodes can be used as rails to develop an integrated and relatively high-throughput platform. Nevertheless, this approach is very sensitive to droplets internal conductivity, and therefore to salt concentration. Moreover, this approach is limited to sandwiched droplets. Electrowetting on dielectric device (EWOD) was also extensively used for droplets transportation, fusion and splitting on digital microfluidic platforms (Sista et al. 2008; Teh et al. 2008). This technique is based on a surface tension shift from hydrophobic to hydrophilic state, by applying a localized voltage between the liquid and a dielectric layer. Integrated electrodes offer a high level of system reconfigurability. Nevertheless, this technology requires rather complex and expensive microfabrication processes that may limit its use. Light actuation was also used to manipulate droplets (Baigl 2012). It provides a contactless approach; it is easily tunable and offers high spatial and temporal resolutions. The conversion of light energy into droplet motion or deviation can rely on different mechanisms such as optical confinement, optoelectrowetting, thermocapillary and chromocapillary effects. The latter was successfully developed by Diguet et al. (2009). The authors have shown that Marangoni flows can be generated by light illumination in order to create a change in the interfacial tension, thus leading to the deviation of microlitre droplets under UV and blue light. More recently, Fradet et al. (2011) developed a microsystem based on laser actuation. Topological modifications in the channel were used to guide sandwiched droplets along complex trajectories or trap them in a microchamber using etched patterns. The combination of these patterns with an external laser allows the selective modification of the trajectory of the droplets and their merging. As a main limitation, however, in the devices mentioned above based on electrodes or topological approaches, the droplets must be sandwiched in order to be guided. Therefore, the dimensions of the microdevices have to be adapted to the droplet sizes or vice versa. This represents a clear limitation whether the size of the droplets used in the microfluidic device is not constant or not known a priori.

The use of magnetic forces for particles manipulation such as magnetophoresis, particle mixing or magnetic capture was extensively described in particular for monophasic microfluidic applications (Van Reenen et al. 2014; Cao et al. 2014). The combination of droplets and magnetic particles represents an important strategy for biological applications, since magnetic fields do not interfere with chemical and biological reactions, and they are much less prone

to induce heating than electric fields. Also, biological fluids can vary largely in conductivity, but share a low and rather uniform magnetic susceptibility, so magnetic manipulation can be performed very robustly in a wide variety of fluids. Indeed, magnetic particles are extensively used as a solid support for capture, purification, extraction or reactions. They have opened the route for many bioanalytical applications within microfluidic tools (Lacharme et al. 2009). The use of magnetic forces was also investigated for the manipulation of droplets (Lehmann et al. 2006). Several approaches were reported using integrated microcoils (Nguyen et al. 2006) or external permanent magnets (Long et al. 2009). Magnetic particles can be extracted and transferred from droplet to droplet in order to perform multistep analyses within microchannels (Ali-Cherif et al. 2012) or using EWOD systems (Wang et al. 2007). Magnetic droplets were also manipulated on open superhydrophobic surfaces using a permanent magnet (Ohashi et al. 2007), but to the best of our knowledge, there have been no demonstration of selective, directed and individual nanolitre droplet manipulation using magnetic rails.

In order to improve over the above-mentioned limitations, we report a new concept allowing the selective and active handling of individual nanolitre droplets based on integrated magnetic rails for the monitoring of droplet content. This platform relies on a very simple and low-cost fabrication technology based on PDMS casting for microchannel fabrication and doctor blade for the integration of magnetic material. This microfabrication approach avoids most of the laborious techniques used in previous approaches to integrate magnetic substrates on chip, such as photolithography and chemical etching (DeRuiter et al. 2014) or the use of liftoff resist and metal evaporation (Paustian et al. 2014). From the conceptual point of view, we believe that this method offers great capabilities regarding droplets manipulation: the principle of the platform relies on the integration into the PDMS chip of different ferromagnetic designs that generate high and localized magnetic field gradients. These gradients can be easily tuned using an external magnetic coil. They modify the energy landscape in the device by creating local attraction areas. The droplets motion in the device thus result from the balance between the oil hydrodynamic drag forces that induce droplets motion and the magnetic rail design that induce deflection of the droplets from their original trajectories and provide a deterministic positioning of the droplets. The rails can be activated on demand, providing the capability to synchronize the droplet position relative to the rail and thus to perform addressing at the individual droplet level. The principle of this magnetic guidance is illustrated in Fig. 1.

We have recently demonstrated that the use of magnetic particles in droplets offers many advantages to perform complex analytical workflows involving capture and
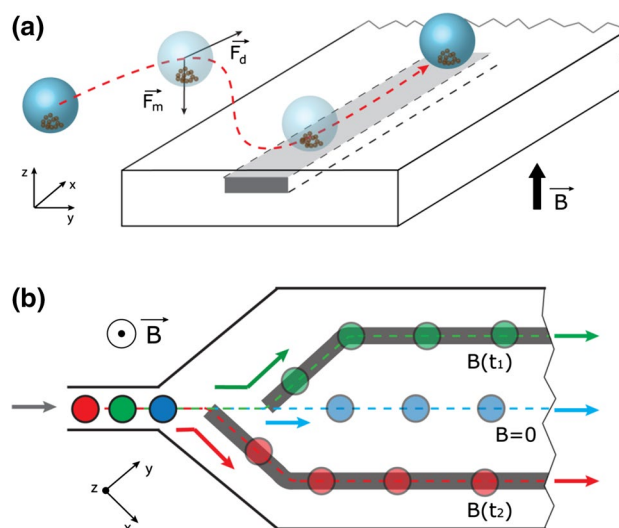

Fig. 1 a Schematic representation of a droplet (*blue sphere*) containing magnetic particles guided by the magnetic rail (*black dotted lines*). The external magnetic field B induces the magnetization of the rail, leading to the attraction of the particles and therefore of the droplet towards the surface of the rail. The droplet is thus pushed by the drag force (F_d) and simultaneously kept along the rail because of the generated magnetic force (F_m). **b** A train of three droplets are entering a chamber having two different magnetic rails. By turning ON and OFF the magnetic field it is possible to choose the droplet to drive in each direction: the first (*blue*) droplet is not driven as B is OFF upon its arrival. The red and green droplets can be directed along two different rails, by turning ON the magnetic field at two different instants (t_1 and t_2) synchronized with the arrival of the chosen droplet over the corresponding rail

extraction operations (Ali-Cherif et al. 2012) as well as one-step analyses (Teste et al. 2013). Here, we show that it is also possible to benefit from the presence of magnetic particles in droplets to control their positions and trajectories in a deterministic manner through magnetic actuation. Using this approach, it is possible to address both sandwiched and non-sandwiched droplets individually to perform sorting, parking and merging operations.

In this work, we investigated the parameters influencing the guidance (magnetic field applied, oil flow rate and geometry of the device) in order to characterize the microfluidic system. Numerical simulations were performed to evaluate hydrodynamic and magnetic forces distribution. A phase diagram describing the operating conditions of magnetic guidance was proposed. Then, we demonstrated the possibility to sort, park and isolate droplets at very precise locations within trapping structures. Droplets merging operations were subsequently triggered at the same time with high temporal resolution. As a demonstration, we applied the developed microfluidic device to parallel enzymatic reactions. We believe that this simple technology will be easily transposable to the study of reaction kinetics, cell culture and bioanalyses for very low amount of samples.

2 Materials and methods

2.1 Device fabrication

Microfluidic devices were fabricated using a combination of conventional PDMS (Sylgard 184, Dow Corning) casting and replica moulding techniques (McDonald and Whitesides 2002). The device was composed of two parts. The bottom part of the device integrates the magnetic rail structures. They were obtained using a "doctor blade" technique (Sayah et al. 2005): first, PDMS pre-polymer (Sylgard 184, Dow Corning, 1:10 base to curing agent ratio) and ferromagnetic iron particles (6–8 μm, Goodfellow) were mixed together (50:50 w/w). Second, this mixture was poured on an aluminium master prepared by micromilling (Minitech Machinery Mill system) and patterning with 200-μm-wide and 200-μm-deep channels that define the rail geometry (Fig. 2a). After degassing, the excess of magnetic PDMS was removed using a soft silicone blade in order to keep the recessed area of the master mould filled with the magnetic polymer (Fig. 2b). At this point, a conventional PDMS pre-polymer mixture was poured on the master (Fig. 2c) and the whole system was kept in an oven at 70 °C for 15 h until reaching the complete curing. The resulting structures were carefully peeled off from the master (Fig. 2d). They consist in a flat PDMS layer of few millimetres with protruding

micrometre magnetic structures (200 μm in height). Finally, the substrate surface was planarized by pouring fresh PDMS on the structures using a silanized glass slide. A stack of adhesive tapes (50 μm thick each one, 3 M) was used as a spacer in order to provide a simple and straightforward fabrication process. All the obtained structures were then kept at 70 °C for 2 h (Fig. 2e). Control experiments were performed to evaluate the reproducibility of the dimensions for the resulting structures. In particular, we performed measurements on sample cross-cuts using optical microscopy followed by image analysis. Results obtained showed a satisfactory reproducibility with a mean thickness of 50 μm (CV of 5 %) for the final PDMS layer on top of the rails.

The top part of the device consists in a microfluidic chamber used for oil and droplets handling. It was obtained by pouring casting PDMS on an aluminium master designed with 3-mm-wide, 5-cm-long and 400-, 500- or 600-μm-high structures (Fig. 2g). The droplets trapping experiments were performed using similar aluminium masters integrating also trapping structures (300 μm length, 100 μm width, 400 μm deep and 50 μm interspace). The inlet and outlet of the microfluidic chamber were composed of 1-cm-long microchannels with a diameter of 500 μm.

In order to bond the top (Fig. 2g) and the bottom parts (Fig. 2h), both surfaces were treated with oxygen plasma (Diener Pico, 100 W, 30 s). Teflon tubings (600 μm OD and
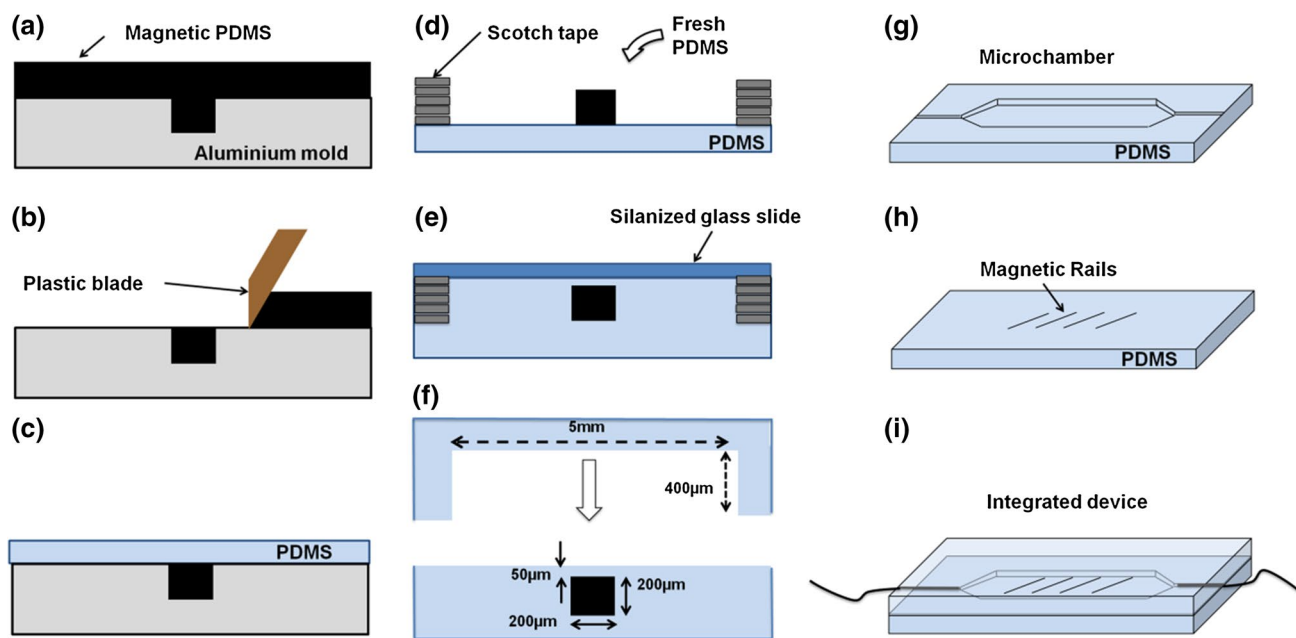

Fig. 2 Workflow of the device microfabrication. In order to produce the *bottom part* integrating the magnetic rails, magnetic PDMS was spread on the aluminium mould (**a**). The excess of magnetic PDMS was removed through doctor blade technique (**b**). Standard PDMS pre-polymer was spread on top of the mould and all the structure was put at 70 °C for 1 h (**c**). The replicated structures were peeled off and planarized by spreading fresh PDMS using silanized glass slides and scotch tape as spacer (**d**, **e**). The resulting *bottom part* integrating the magnetic rail was bonded with the microchamber (**f**). **g**, **h**, **i**) Scheme showing the cross section of the microchamber, the rails and the final device, respectively. The final device was plugged with Teflon tubings at the inlet and outlet

300 µm ID, Sigma-Aldrich) were then inserted in the inlet and outlet of the microdevice (Fig. 2i). Finally, the internal chamber surface was treated by 1H,1H,2H,2H-perfluorodecyltrichlorosilane (100 µL in 1 mL of FC-40 oil) for 1 h to improve oil wetting and thus droplet stability.

2.2 Droplet generation

Aqueous droplets containing 1-µm magnetic beads (Myone, Invitrogen) at 40 µg/µL (10^6 magnetic beads per droplet) were generated by sequentially aspirating 35 nL of an aqueous suspension of magnetic beads and fluorinated oil (FC-40, 3 M) mixed with PEG-Di-Krytox surfactant at 2 % (w/w) (Holtze et al. 2008) in Teflon tubing (300 µm ID and 600 µm OD, Sigma-Aldrich). Fluid handling was performed using syringe pumps (Cetoni GmbH) and a 1-mL syringe (internal diameter of 0.4 mm); the droplets were injected in the microfluidic device at different flow rates varying from 2 to 10 µL/s.

2.3 Magnetic field control

The microdevice was inserted in a home-made electromagnetic coil (5.5 cm ID,13.5 cm OD and 4.5 cm height) fabricated with 0.8-mm electrically insulated copper wires and driven by a tunable power supply (0–3 A, 0–25 V). This system allows the generation of a homogeneous magnetic field in the centre of the coil, with an orientation aligned along the coil axis. The field intensity can be tuned arbitrarily from 0 to 45 mT in the 0–3 A current operating range.

2.4 Droplet guidance and parking

Droplets were sequentially injected in the microchamber. When the first droplet passed over the chosen rail, the external magnetic coil was turning ON till the droplet was parked in the corresponding trap. Then, the magnetic coil was turning OFF until a new droplet was introduced in the microchamber. The same procedure was repeated for the whole droplets train.

2.5 Magnetic beads functionalization

Peroxidase grafting consists in mixing 400 µL of magnetic beads at 10 mg/mL, 100 µL of 1-ethyl-3-(3-dimethylaminopropyl) carbodiimide at 2 mg/mL, 100 µL of N-hydroxysulphosuccinimide at 6 mg/mL and 1 mL of peroxidase from horseradish at 1 mg/mL. After overnight incubation at 4 °C, magnetic beads were rinsed 5 times and redispersed in PBS buffer.

To prevent non-specific adsorption, 400 µL of magnetic beads at 10 mg/mL were coated with 1 % BSA (w/v). After overnight incubation, magnetic beads were rinsed 5 times and redispersed in PBS buffer.

2.6 Droplet merging and enzymatic reaction

Four droplets (35 nL internal volume) containing Amplex Red substrate (100 µM) and 10^6 magnetic beads grafted with peroxidase were sequentially stored within the traps. Then, a second set of four 35-nL droplets containing 10^6 magnetic beads coated with BSA and various concentrations of H_2O_2 (from 0 to 200 µM) were sequentially transported in the four traps. The concentration of the surfactant in the oil was tuned at 2 % (w/w) so that once stored, each couple of droplet could be kept stable in each trap. Droplet merging could be achieved by increasing the flow rate at values higher than 15 µL/s. In such case, the hydrodynamic drag force was found to be sufficient to induce coalescence. Once merged, the fluorescent product of the enzymatic reaction was measured over time every 5 s using an inverted microscope (Nikon) equipped with a mercury lamp and Cy3 spectral filters (excitation wavelength: 530–560 nm and emission wavelength: 573–648 nm).

3 Results and discussion

3.1 Demonstration of magnetic guidance

The droplets generation and manipulation were performed with the experimental set-up described in (Figure S1 online resources). The microsystem was inserted in the centre of the electromagnetic coil, where the magnetic field is homogeneous and oriented perpendicularly to the (x,y) plane. In this configuration, the magnetic particles within the droplet behave as small magnets with a magnetization oriented along the magnetic field direction. Even in the absence of magnetic rails, they spontaneously self-assemble into 1D columns in the droplet. This process does not modify the shape and hydrodynamic behaviour of the droplet. Moreover, as the magnetic flux density is homogeneous in the microdevice, the magnetic gradient in the (x,y) plane is negligible meaning that the magnetic force that may impact the droplet trajectory can also be neglected. This hypothesis was confirmed experimentally by monitoring the trajectories of droplets while switching ON and OFF the electromagnetic coil. The selective transport and guidance of magnetic droplets is based on the activation of ferromagnetic rails by an external electromagnetic coil. Although the microdevice is placed in a homogeneous magnetic field, the presence of the ferromagnetic rails locally modifies the magnetic field distribution thus resulting in a magnetic field gradient (∇B) that modifies the energy landscape at the vicinity of the rails. This mechanism gives rise to a magnetic force (F_m) on the magnetized particles within the droplet. The trajectory of the mobile droplets results from a balance between hydrodynamic drag and magnetic
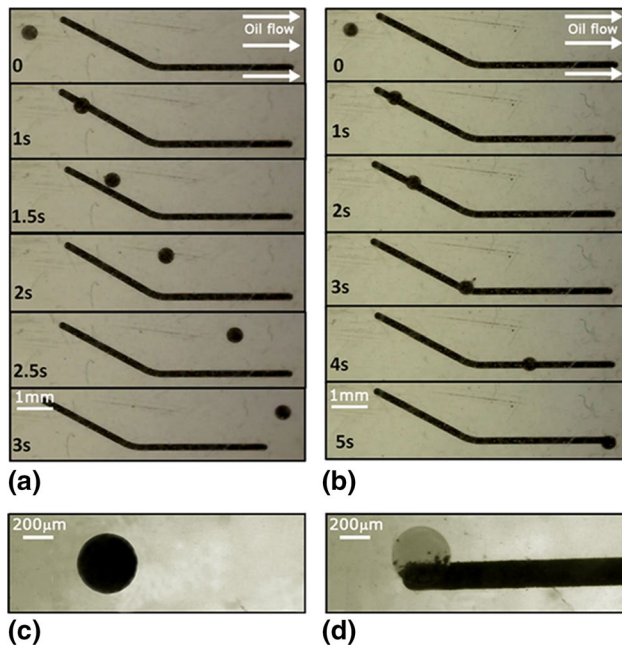
Fig. 3 Images sequences showing the trajectory of droplets loaded with 1-μm superparamagnetic particles at 40 μg/μL (around 10^6 magnetic particles), with external magnetic field turned OFF **a** and ON **b**. The *arrows* indicate the orientation of the oil flow. The flow profile velocity is homogeneous across the width of the chamber. Particle spatial distribution in the droplet when the magnetic field is turned OFF (**c**) (particles are homogeneously dispersed) and when it is ON (**d**) (particles are confined and form a cluster above the rail)

guidance forces. The rail geometry used for the first proof of concept experiments consisted in a 200-μm-wide and 5-cm-long bent track (Fig. 3). The oil flow rate was set at 5 μL/min.

Image sequences showing the trajectory of droplets in the device are shown in Fig. 3. When the external magnetic field was switched OFF, the droplets were dragged by the oil flow with a linear trajectory (Fig. 3a). Conversely, in the presence of the external magnetic field, magnetic droplets experience a magnetic attraction force when passing over the ferromagnetic rails. The magnetic rails induce a confinement force that results in the deviation of the droplet from its original trajectory (Fig. 3b). It is important to notice that the flattening process avoids any guidance effect induced by topographically modified surfaces as previously demonstrated by Dangla et al. (2011). Moreover, the diameter of the droplet was maintained slightly below the microchannel height so that the channel surface did not interfere with droplet motion.

Careful observations of the droplets show that upon guidance, the rails induce an attractive force that leads to the confinement of the suspended magnetic particle into a cluster (Fig. 3d). This effect was not observed in the absence of magnetic field, as shown in Fig. 3c. In

the absence of magnetic structures, the droplet follows a straight trajectory when the coil is turning ON since the magnetic particles are submitted to a homogeneous magnetic field (data not shown).In contrast to our previously published work (Ali-Cherif et al. 2012), the formation of this cluster was not sufficient to induce the extraction of the particles from the droplet. The magnetic force induced by the rail is energetically not sufficient to destabilize the droplet interface and induce droplet splitting. These observations were in good agreement with magnetic forces and surface energy calculations (supporting material). This shows that the magnetic force exerted on the particles cluster is directly transferred to the droplet without affecting its stability. The droplet thus behaves as a mobile reservoir with properties comparable to those of a magnetic particle ensemble.

3.2 Physical background

Droplet guidance along the magnetic rails results from the balance between different forces acting on the droplets. It is interesting to distinguish in-plane forces (x,y plane) from vertical forces (z axis) as summarized in Fig. 4.

We first considered the motion of the droplet along the vertical component (z axis).

The sum of the forces acting on the droplets on the z axis (F_z) is given by

$$\sum \overrightarrow{F_z} = \overrightarrow{F_b} + \overrightarrow{F_g} + \vec{F}_m \tag{1}$$

with F_b the buoyancy force, F_g the gravitational force and F_m the magnetic force acting on the particle cluster.

When no external magnetic field is applied, the movement of the droplet along the z axis is only defined by F_b and F_g. As the oil density ($d = 1.85$ g/cm^3) is higher than the aqueous phase density ($d = 1$ g/cm^3) within the droplet, F_b pushes the droplet towards the top of the chamber, away from the magnetic rails.

In the presence of the external magnetic field, the resulting magnetic force F_m and the relative magnetic energy E_m are given by the following simplified equations (Online resources 1 for more details):

$$\overrightarrow{F_m} = \frac{Q}{\rho} \overrightarrow{M} \nabla(\vec{B}) \tag{2}$$

$$E_m = -(\vec{m} \cdot \vec{B}) \tag{3}$$

with Q the mass of magnetic particles (g) in the droplet, ρ the magnetic beads density (g/m^3), M the magnetization (A/m), $\vec{m}$ the magnetic moment (A/m^2), $\vec{B}$ and ∇B the magnetic flux density (T) and its gradient (T/m), respectively.

COMSOL simulations were used to estimate the magnitude and orientation of B, ∇B, E_m and F_m that are applied

Fig. 4 Description of the balance of forces acting on the magnetic beads in the droplet in (**a**) the (*y,z*) plane and (**b**) (*x,y*) plane. **c** Calculation of the magnetic forces on the *y* component F_{my} around the rail. **d** Calculation of the magnetic energy on the *y* component E_{my} around the rail. Simulations were performed by considering a fixed *z* value at 50 μm above the rail, which corresponds to the PDMS thickness from the flattening step. The *dashed lines* in the F_{my} and E_{my} graphs show the edges of the rail. *red*, *green* and *blue curves* correspond to 1 (15 mT), 2 (30 mT) and 3 A (45 mT) applied in the coil, respectively
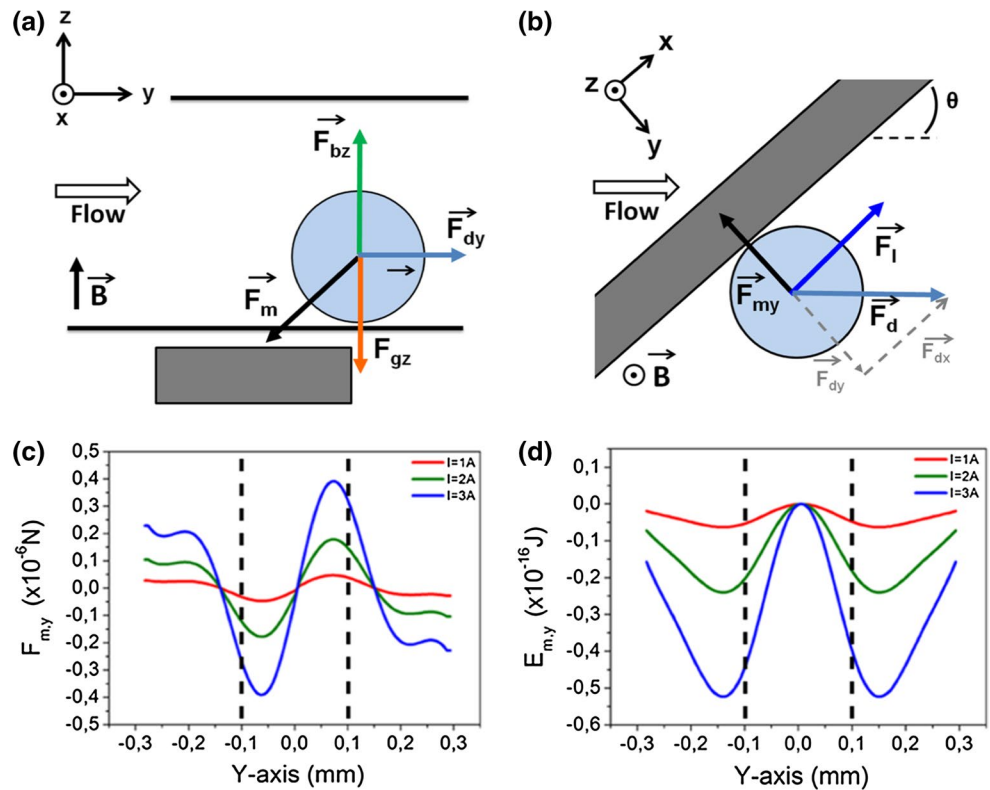
on the micrometric particles confined in the water droplet. Calculations were based on the measured magnetization curves of the particles and on the geometry of the microfluidic device.

Although the magnetic field distribution is homogeneous within the coil, as expected, simulation results show that the external magnetic field distribution and the energy landscape are modified in the presence of the magnetic rail. The magnetic field lines are focused towards the magnetized rail (Online resources, Figure S2), thus resulting in a local increase in the B_z value associated with a magnetic field gradient oriented towards the magnetic rail. As a consequence, F_{mz} vectors are oriented towards the rails, so that the magnetic cluster and therefore the droplets are attracted to the surface of the rail. The intensity of F_{mz} was estimated from 4 to 6 μN for current values ranging from 1 to 3 A, respectively (data not shown). The buoyancy force F_b was estimated at 0.28 μN. Thus, even for the lowest current value applied at the coil (1 A), the magnetic force is sufficient to counter balance the influence of buoyancy, bringing the droplet close to the rail (an oil wetting layer of a few micrometres is maintained between the droplet and the surface, by the combination of surface tension contrast and hydrodynamic lubrication layer).

We further investigated the in-plane (*x,y*) forces acting on the droplet and causing changes in its trajectory (see Fig. 4b). It should to be mentioned that the friction forces was neglected in order to simplify our forces model,

but will be discussed further in this paragraph. The droplet is subjected to a drag force from the oil flow described as $F_d = 6\pi \eta r \Delta v$ [where η is the viscosity of water (Kg s^{-1} m^{-1}), r the droplet radius (m) and Δv the difference between fluid and droplet velocity (m s^{-1})]. Droplet trajectories are also influenced by the in-plane component of the magnetic force (F_m), which is only oriented along the *y* axis. Indeed, if we consider a long rail with a width w and a length *l*, with $l \gg w$, then the magnetic field gradient ∇B can be neglected along the *x* axis. In order to evaluate the potential influence of wall effect lift and shear-gradient lift forces on the droplet trajectory close to the walls, we investigated the flow velocity profile using COMSOL simulations (Figure S3 online resources). We observed that, except for the regions located at the vicinity of the walls, the flow intensity is almost constant across the channel, in a direction perpendicular to the fluid flow. This result indicates that in the region where the guiding occurs, the influence of both wall effect lift and shear-gradient lift forces can be neglected and that the flow profile has a negligible influence on droplet trajectories during lateral migration.

Figure 4c and d shows the evolution of F_{my} and E_{my} along the *y* axis, calculated following Eqs. 2 and 3 for three different current values and for a *z* position 50 μm above the rail. The E_{my} curves show two energy minima located at the edges of the rail, which correspond to stable positions for the magnetic cluster. As expected, increasing the current in the coil corresponds to an increase in the attractive force

in these regions and thus a decrease in E_{my}. According to these results, the cluster and therefore the droplet should be preferentially confined at 0.15 or −0.15 mm from the centre of the rail in the absence of drag force. Considering the balance of forces on the (x,y) plane, the resulting force (or lateral force, F_l), acting on the droplet, can be written as:

$$\overrightarrow{F_l} = \overrightarrow{F_m} + \overrightarrow{F_d} = (F_d \cos\theta)\overrightarrow{e_x} + (F_m - F_d \sin\theta)\overrightarrow{e_y} \quad (4)$$

with θ the angle between F_d and the rail axis.

In order to ensure the guidance of the droplet above the rail, the following condition has to be satisfied: $F_{my} > F_d \sin\theta$. In such conditions, the droplet will be pushed and transported along the x direction and along the rail. On the contrary, if $F_{my} < F_d \sin\theta$, the droplet is disengaged from the magnetic rail and is dragged away by the oil flow. It is also interesting to notice that according to Eq. 4, increasing angle θ requires an increase in the F_m value to keep a magnetic confinement on the rail sufficient to compensate for hydrodynamic drag. We compared these theoretical assumptions with experiments. The results are commented in the next paragraph.

As mentioned earlier, friction forces were neglected in our model since the influence of these forces that may arise at the vicinity of the magnetic rails is difficult to investigate. Some studies have been proposed in the literature to investigate the motion and velocities of droplets or bubbles within microchannels according to their degree of confinement (Baroud et al. 2010; Fuerstman et al. 2007; KopfSill and Homsy 1988). These experiments were performed either in fully confined geometries or in Hele-Shaw chambers and have shown that the velocity of droplets or bubbles is lower than the oil flow and closely dependent on the surfactant concentration. Our case is intermediate since the droplets do not experience a confinement due to the device geometry, but only an attractive magnetic force towards the integrated magnetic rails. Our work is thus a particular case where the droplet is partially confined in one direction. Nevertheless, experimental observations also revealed that for an average flow rate of 5 μL/s, the oil flow velocity in the chamber is 4×10^{-3} m/s, while the droplet velocity in the absence or presence of the field was 2.57×10^{-3} and 0.52×10^{-3} m/s, respectively. These results are in good agreement with the work mentioned previously (KopfSill and Homsy 1988) and confirm the presence of frictional forces. Modelling these frictional forces would require additional experiments that go beyond the scope of this work and it is important to mention that, in our specific case, even if the presence of friction forces may impede the droplet velocity during guiding, it should not affect the balance of forces (drag force vs magnetic force) involved in the efficiency of the trapping and guiding mechanisms.

3.3 Operating conditions for droplet guidance

In order to validate the analytical model proposed above, phase diagrams showing the experimental conditions that verify $F_{my} > F_d \sin\theta$ are given in Fig. 5. In these experiments, the droplet size and the magnetic beads quantity were kept constant, while B, θ as well as the oil flow rate were varied in order to study the influence of F_m, $\sin\theta$ and F_d, respectively. B varied from 0 to 45 mT, θ from 15° to 45° and oil flow rate from 2 to 10 μL/s corresponding to
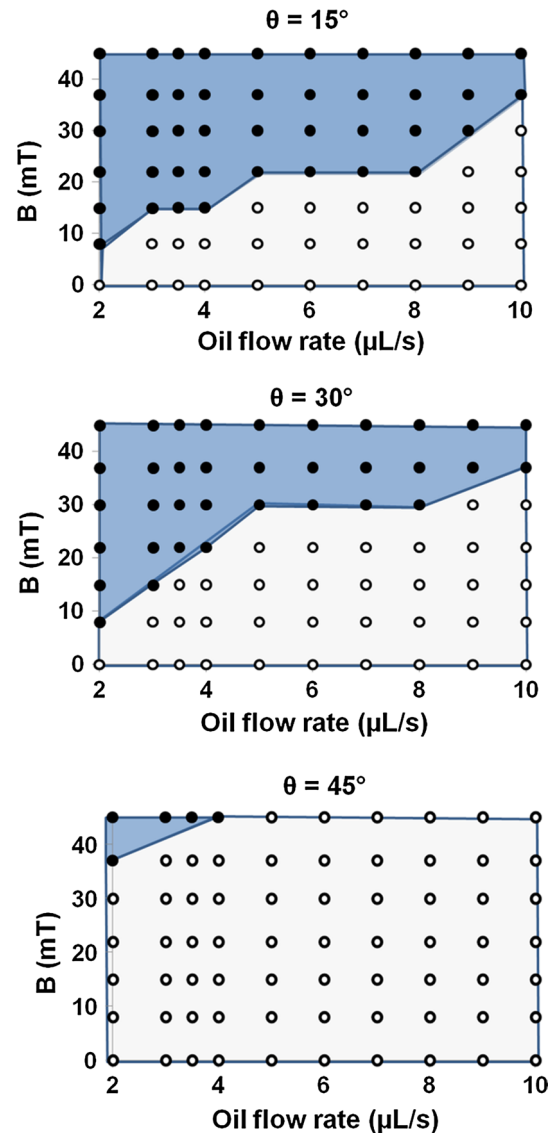

Fig. 5 Experimental phase diagrams obtained varying B, θ and the oil flow rate. *Blue regions* (*black experimental points*) show the operating conditions giving rise to efficient guidance while droplet disengagement was observed in white region (*white experimental points*). Droplets with a diameter of 400 μm and loaded with 1.5 μg (10^6 magnetic particles) of 1 μm magnetic particles were introduced in a 600 μm height chamber

a variation of flow speed from 1.6 to 8.2×10^{-3} m/s. As expected, two different regimes were identified: (1) droplets were guided all along the rail (blue region) and (2) droplets disengaged from the rail (white region). As a general trend, all phase diagrams clearly show that increasing the flow rate and thus F_d, the magnetic field has to be increased in order to provide a F_m sufficient to lead to an effective guidance along the rail.

The influence of the rail orientation relative to the flow stream direction is also clearly observable. By comparing all diagrams, we can observe that the effective guidance window (blue region) decreases when θ increases, as estimated by our model (see Eq. 4). In other words, large deviation from the original droplet trajectory has to be counterbalanced by an increase in the magnetic field intensity. For θ values above 45°, the maximum magnetic field provided by our electromagnetic coil (around 45 mT) was not sufficient to maintain the guidance even for flow velocities down to 2 μL/s (flow speed of 1.6×10^{-3} m/s).

Contrary to previously reported methods (DeRuiter et al. 2014; Fradet et al. 2011), the guidance mechanism involved in this approach does not require any confinement of the droplet (sandwiched drops constrained by the top and bottom boundaries). As a matter of fact, droplets with a diameter of 400 μm (35 nL) were efficiently transported along the rails in a chamber of height up to 600 μm. Interestingly, experiments performed with slightly confined droplets (400-μm droplet and 400-μm-high chamber) did not show any influence of friction forces that could prevent droplets guiding along the rail.

Moreover, the smallest quantity of magnetic beads required to obtain an efficient guidance along the rails was 1.5 μg (10^6 magnetic beads), and the smallest droplet volume tested in this work was 35 nL (400 μm in diameter). These results highlight the flexibility achievable with this platform in terms of droplet volumes and solid contents.

The concepts investigated in this study were validated for 400-μm droplets (35 nL), but they seem to be applicable to smaller droplets. Keeping constant the magnetic field, the main parameter influenced by a change in the droplet diameter is the drag force F_d that scales with the radius of the droplet. Decreasing the radius of the droplet while keeping the same particle content pushes the forces balance towards the magnetic confinement. This argument is valid as long as the total volume of particles is lower than the droplet volume itself. With a particle content of 10^6 particles, it is possible to consider droplets with a diameter down to 100 μm (size of the cluster for 10^6 particles). The distance between the droplet and the rail that increase for small droplets does not impede the trapping and guiding process. Indeed, if we consider a droplet of 100 μm located at a maximal distance of 300 μm above the rail (considering a microchamber of 400 μm height), simulations performed for 10^6 particles within the droplet suggest a magnetic force on z axis at about 800 nN which is above the buoyancy force (about 280 nN) thus meaning that trapping mechanism is still efficient. The maximum amount of particles scales with R_d^3 (R_d radius of the droplet), meaning that the magnetic force would decrease quickly with the droplet size. As a consequence, the validation of the trapping mechanism for droplets below 100 μm (5 nL) would require a specific study and experimental validation that goes beyond the scope of this study.

3.4 Droplet sorting, parking and merging

The advantage of the proposed technology is the possibility to activate and deactivate on demand the guidance properties of the ferromagnetic rails, by simply turning ON and OFF the external magnetic field. This approach offers the opportunity of addressing individually droplets by a temporal synchronization of the rail activation with the droplets position and thus to potentially control the trajectory of each droplet entering in the device. A proof of concept of the individual droplets sorting was performed in the device described in Fig. 6.

The traps are composed of out-of-plane structures that allow the oil to flow through but induce an increment of hydrodynamic resistance sufficient to drive the main flow streamlines around the structures. The dimension and position of the traps have been optimized through COMSOL hydrodynamic simulations to prevent droplet trapping in the absence of magnetic field (Online resources Figure S4 and video S1).

By turning ON the external magnetic field while the droplet passes over the desired rail, it is possible to deviate droplets from their initial trajectory and to drive them along the rail until they reach the inner part of trapping structures. Experiments show that in this configuration, the magnetic confinement force is sufficient to compensate for the flow deviation around the structures and push the droplets into the traps. COMSOL simulations were used to investigate the flow velocity profile around the trapping structures. As shown in the figure S4 (online resources), the pillars composing the trap deviate the fluid flow and induce a lateral flow with a maximum velocity around 5.10^{-3} m/s for an average flow rate of 5 μL/s. The corresponding drag force on the droplet is about 3.8 nN and is well below the magnetic force submitted by the droplet in the y direction which vary from 50 to 400 nN (for current values from 1 to 3 A).

As shown on Fig. 6, the first droplet is sorted and parked in the trap 1 by turning ON the magnetic field when the droplet passed over the rail r1. Once the droplet is immobilized, the magnetic field can be switched OFF, while the drag force exerted on the droplet keep them in a stable position in the trap. Following a similar procedure, the
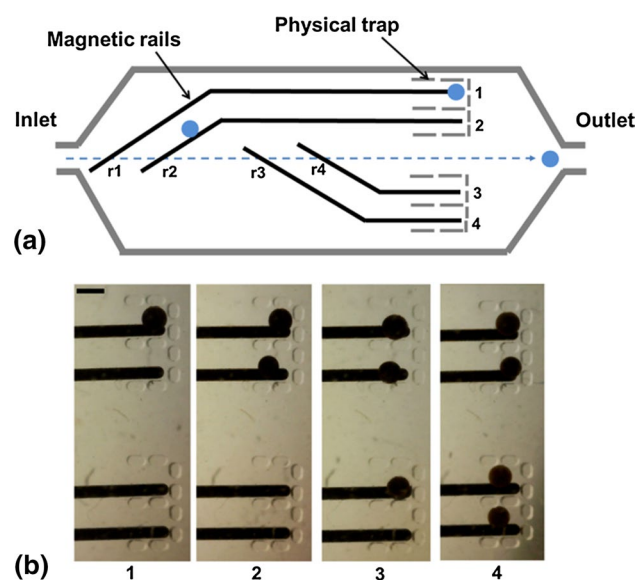
Fig. 6 a Schematic view of the microdevice combining a magnetic rails network and a physical traps array. Droplets were generated and injected into the chamber using a syringe pump at a constant flow rate (5 μL/min). The rails (*r1* to *r4*) were sequentially activated allowing the guidance and parking of the droplets individually in four different traps (*1–4*). The *dashed lines* represent the droplet trajectory in the absence of magnetic field. **b** Images show the sequential and selective droplet parking from *trap 1* to *trap 4*. The *scale bar* is 400 μm

Fig. 7 Images sequence of droplets merging and mixing. **a** A first droplet of 50 nL containing a *yellow dye* was guided and parked. **b** A second droplet of 35 nL containing purple dye was transported and parked to the same trap. **c** A flow rate higher than 15 μL/s was applied to induce merging and, **d** complete mixing was observed after 4 s

following droplets could sequentially be sorted and stored from trap 2–4 by sequentially activating r2 to r4 (Online resources video S2 and S3). By reversing the flow, droplets can be released from the traps for collection. Interestingly, by reversing the flow and keeping the field ON, the droplet can also be returned back to the inlet streamline (results not shown).

As all rails are activated simultaneously, one limitation arises from the fact that the rails have to stay active all along the droplet trajectory, until the droplet is stored in the appropriate trap. During this time frame, it is not possible to modify the status of the field and to process differently a new incoming droplet. The processing throughput is thus limited by the droplet speed, i.e. by the flow velocity. Here, complete guiding and storing steps were carried out with a throughput of 4 droplets/minute. Fast processing time can be achieved with higher flow rate and stronger magnetic power given the same trajectory length.

The same procedure can be advantageously used to perform a selective merging of droplets (Fig. 7a–d). After immobilizing a first set of droplets, a second train of droplets can be introduced in the device and transported to the traps where a first droplet was stored. Once in contact, droplets located in the same trap can be kept intact and further merged by increasing the flow velocity. In our device, we observed that droplet merging was occurring for flow
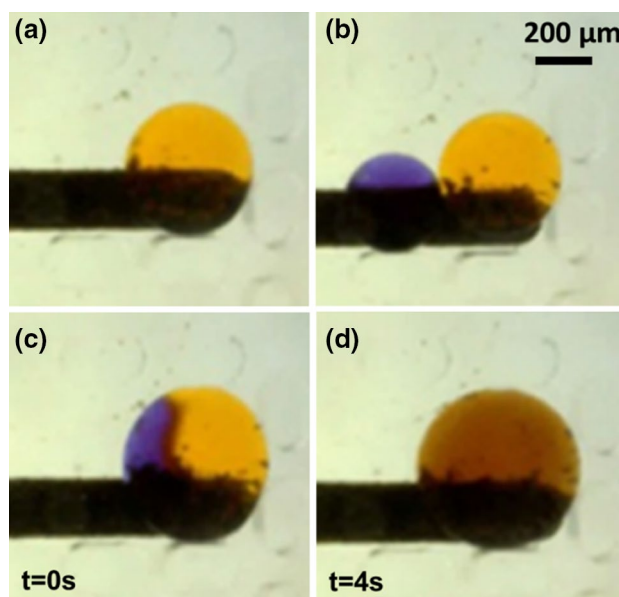
rate higher than 15 μl/s (flow speed of 12.10^{-3} m/s), which corresponds to a F_d exerted on the second parked droplet of 31.4 nN. Above this threshold value, the hydrodynamic drag force exerted on a drop is sufficient to merge droplets and overcome the droplet stabilization effect provided by surfactants in the oil. In this geometry, passive diffusion is sufficient to mix the content of two droplets in $t < 5$ s. If a more efficient mixing is needed, the magnetic beads within the droplet can be used as an active micromixer by periodically turning ON and OFF the magnetic field (Online resources video S4).

3.5 Parallel enzymatic reactions

As a final proof of concept, we performed enzymatic reactions to demonstrate the capabilities of the microdevice to monitor chemical reactions and to extract accurate information from individual droplet (Fig. 8). We chose a well-known system based on a peroxidase that cleaves the Amplex Red substrate into fluorescent Resorufin in the presence of H_2O_2. This system is usually used to measure H_2O_2 release from cells. A first set of four droplets containing the same quantity of magnetic beads coated with peroxidase enzyme (corresponding to an enzyme concentration of 65 fM within the droplet) and Amplex Red (100 μM) were guided and stored individually in each trap. The same procedure was repeated with a second set of droplets containing different concentrations of H_2O_2 ranging from 0
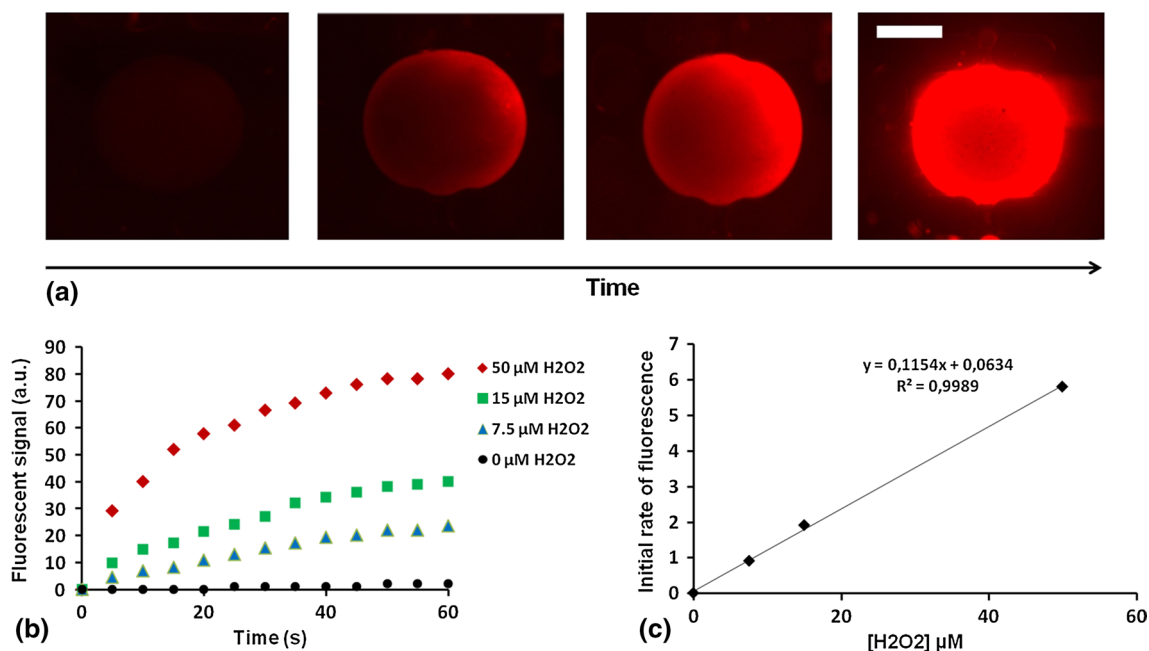
(a)   **Time**

(b)   **(c)**

Fig. 8 **a** An example of fluorescent signal increase over time after droplets merging for a fixed enzyme (65 fM), Amplex Red (50 μM) and H_2O_2 (50 μM) concentration. The *scale bar* is 200 μm. **b** peroxidase reactions kinetics in the fused droplets for four different H_2O_2 concentrations keeping enzyme (65 fM) and Amplex Red (50 μM) substrate constant. **c** Calibration curve for the determination of H_2O_2 within droplets

to 100 μM (i.e. from 0 to 50 μM final concentration after droplets merging). The second set of droplets was manipulated by including in each droplet "biologically passive" magnetic particles coated with BSA to prevent non-specific adsorption. Droplets merging was induced simultaneously on all droplets by increasing the flow rate up to 15 μL/s (F_d = 31.4 nN). The four different independent reactions were monitored in parallel by measuring droplets fluorescent signal over time (Fig. 8a,b). First, the fluorescence increases with time at the beginning of the reaction then reaches a plateau. The non-specific fluorescent signal was measured with a droplet containing no H_2O_2; in this condition, no fluorescent signal was detected.

The enzyme kinetics of fluorescent Resorufin product formation is governed by Michaelis–Menten equation (Eq. 5) (Copeland 2000).

$$V_i = \frac{V_{max} \times [S]}{[S] + K_m} \qquad (5)$$

where V_i is the initial reaction velocity, V_{max} the maximum reaction velocity, K_m the Michaelis–Menten constant and [S] the substrate concentration.

In our experimental conditions, the substrate concentration was small as compared to K_m value (Kengen et al. 2001) (peroxidase K_m value for H_2O_2 is 850 μM); therefore, V_i is proportional to H_2O_2 concentration (Berg et al. 2002). In our study, the initial reaction velocity corresponds to the

initial rate of fluorescence, i.e. the slope of each reaction curves. The rates of fluorescence were 0, 0.9, 1.92 and 5.8 for 0, 7.5, 15 and 50 μM H_2O_2 concentrations, respectively. The relative standard deviation was calculated to be 13 % based on three repetitions. The reported calibration curve for the determination of H_2O_2 concentration is shown in Fig. 8c. It represents the evolution of initial rate of fluorescence as a function of H_2O_2 concentration.

4 Conclusion

In this work, we showed that the integration of miniaturized magnetic rails opens a novel way to manipulate droplets in microfluidic devices. We demonstrated the ability of the device to perform a sorting, trapping and merging sequence by combining a magnetic rails network together with trapping structures placed at the extremity of each rail. This device can perform parallel chemical reactions that can be critical for multiple analytical and diagnostic procedures. We think that this platform offers an efficient alternative to more complex and expensive digital microfluidic devices, especially for applications that do not require high throughput, because of the following advantages: (1) simplicity of fabrication and use, (2) low cost, (3) selective manipulation of individual nanolitre droplets, (4) integration of complex operations (guidance, sorting, parking and merging) in a single device and (5) parallel analyses.

The proposed device does not offer the level of flexibility provided by EWOD for droplets handling. Indeed, the integration of electrodes allows step-wise moving control functions that provide more flexibility to manipulate individual droplet and perform merging and splitting functions without the need of hydrodynamic flows. Nevertheless, we think that the developed device is well adapted for simple and continuous processes involving sorting and analysis of nanolitre droplets. The simplicity of design and fabrication processes appear as clear advantages for the fabrication of low-cost analytical platforms integrating droplet generation, sorting and analytical operations. Moreover, magnetic forces have a long interaction range. This system could be easily combined with other magnetic concepts thus paving the way to multiple and complex analytical operations. The necessity of loading each droplet with a magnetic particle amount sufficient to provide guidance may appear as a limitation. Nevertheless, we demonstrated in our previous work devoted to magnetic tweezers that particles can be advantageously used as a support for capture and extraction purposes, thus serving two aims simultaneously. Besides, various magnetic particles with efficient "repulsive" coatings are available in the market, so for most applications, we expect that magnetic particles can be used for guidance without interfering with the process under study inside the droplet. Extraction, purification and capture processes can be advantageously coupled to individual droplet handling for complex bioanalytical processes. Future work will be devoted to the coupling and integration of magnetic rails with magnetic tweezers in order to provide a fully integrated and flexible analytical platform for single-cell analysis.

References

Abate AR, Hung T, Mary P, Agresti JJ, Weitz DA (2010) High-throughput injection with microfluidics using picoinjectors. Proc Natl Acad Sci USA 107(45):19163–19166

Abbyad P, Dangla R, Alexandrou A, Baroud CN (2011) Rails and anchors: guidance and trapping droplet microreactors in two dimensions. Lab Chip 11(5):813–821

Adamson DN, Mustafi D, Zhang JXJ, Zheng B, Ismagilov RF (2006) Production of arrays of chemically distinct nanolitre plugs via repeated splitting in microfluidic devices. Lab Chip 6(9):1178–1186

Ahn K, Kerbage C, Hunt T, Westervelt R, Link D, Weitz D (2006) Dielectrophoretic manipulation of drops for high-speed microfluidic sorting devices. Appl Phys Lett 88(2):024104

Ahn B, Lee K, Lee H, Panchapakesan R, Oh KW (2011) Parallel synchronization of two trains of droplets using a railroad-like channel network. Lab Chip 11(23):3956–3962

Ali-Cherif A, Begolo S, Descroix S, Viovy JL, Malaquin L (2012) Programmable magnetic tweezers and droplet microfluidic device for high-throughput nanoliter multi-step assays. Angew Chem Int Ed 51(43):10765–10769

Baigl D (2012) Photo-actuation of liquids for light-driven microfluidics: state of the art and perspectives. Lab Chip 12(19):3637–3653

Baret JC, Miller OJ, Taly V, Ryckelynck M, El-Harrak A, Frenz L, Rick C, Samuels ML, Hutchison JB, Agresti JJ, Link DR, Weitz DA, Griffiths AD (2009) Fluorescence-activated droplet sorting (FADS): efficient microfluidic cell sorting based on enzymatic activity. Lab Chip 9(13):1850–1858

Baroud CN, Gallaire F, Dangla R (2010) Dynamics of microfluidic droplets. Lab Chip 10(16):2032–2045

Berg JM, Tymoczko JL, Stryer L (2002) Biochemistry, 5th edn. W H Freeman, New York

Cao Q, Han X, Li L (2014) Configurations and control of magnetic fields for manipulating magnetic particles in microfluidic applications: magnet systems and manipulation mechanisms. Lab Chip 14(15):2762–2777

Chabert M, Dorfman KD, Viovy JL (2005) Droplet fusion by alternating current (AC) field electrocoalescence in microchannels. Electrophoresis 26:3706–3715

Churski K, Michalski J, Garstecki P (2010) Droplet on demand system utilizing a computer controlled microvalve integrated into a stiff polymeric microfluidic device. Lab Chip 10(4):512–518

Cohen DE, Schneider T, Wang M, Chiu DT (2010) Self-digitization of sample volumes. Anal Chem 82(13):5707–5717

Copeland RA (2000) Enzymes: a practical introduction to structure, mechanism and data analysis, 2nd edn. Wiley, New York, USA

Dangla R, Lee S, Baroud CN (2011) Trapping microfluidic drops in wells of surface energy. Phys Rev Lett 107(12):124501

DeRuiter R, Pit AM, de Oliveira VM, Duits MHG, van den Ende D, Mugele F (2014) Electrostatic potential wells for on-demand drop manipulation in microchannels. Lab Chip 14(5):883–891

Diguet A, Guillermic RM, Magome N, Saint-Jalmes A, Chen Y, Yoshikawa K, Baigl D (2009) Photomanipulation of a droplet by the chromocapillary effect. Angew Chem Int Ed 48(49):9281–9284

Fradet E, McDougall C, Abbyad P, Dangla R, McGloin D, Baroud CN (2011) Combining rails and anchors with laser forcing for selective manipulation within 2D droplet arrays. Lab Chip 11(24):4228–4234

Fuerstman MJ, Lai A, Thurlow ME, Shevkoplyas SS, Stone HA, Whitesides GM (2007) The pressure drop along rectangular microchannels containing bubbles. Lab Chip 7(11):1479–1489

Holtze C, Rowat AC, Agresti JJ, Hutchison JB, Angilè FE, Schmitz CHJ, Köster S, Duan H, Humphry KJ, Scanga RA, Johnson JS, Pisignano D, Weitz DA (2008) Biocompatible surfactants for water-in-fluorocarbon emulsions. Lab Chip 8(10):1632–1639

Huebner A, Bratton D, Whyte G, Yang M, Demello AJ, Abell C, Hollfelder F (2009) Static microdroplet arrays: a microfluidic device for droplet trapping, incubation and release for enzymatic and cell-based assays. Lab Chip 9(5):692–698

Kengen SW, Bikker FJ, Hagen WR, de Vos WM, van der Oost J (2001) Characterization of a catalase-peroxidase from the hyperthermophilic archaeon Archaeoglobus fulgidus. Extremophiles 5(5):323–332

KopfSill AR, Homsy GM (1988) Bubble motion in a Hele–Shaw cell. Phys Fluids 31(1):18–26

Lacharme F, Vandevyver C, Gijs MAM (2009) Magnetic beads retention device for sandwich immunoassay: comparison of off-chip and on-chip antibody incubation. Microfluid Nanofluid 7(4):479–487

Lehmann U, Hadjidj S, Parashar VK, Vandevyver C, Rida A, Gijs MAM (2006) Two-dimensional magnetic manipulation of microdroplets on a chip as a platform for bioanalytical applications. Sens Actuators B 117(2):457–463

Link DR, Anna SL, Weitz DA, Stone HA (2004) Geometrically mediated breakup of drops in microfluidic devices. Phys Rev Lett 92(5):054503

Long Z, Shetty AM, Solomon MJ, Larson RG (2009) Fundamentals of magnet-actuated droplet manipulation on an open hydrophobic surface. Lab Chip 9(11):1567–1575

Lorenz RM, Edgar JS, Jeffries GDM, Chiu DT (2006) Microfluidic and optical systems for the on-demand generation and manipulation of single femtoliter-volume aqueous droplets. Anal Chem 78(18):6433–6439

McDonald JC, Whitesides GM (2002) Poly(dimethylsiloxane) as a material for fabricating microfluidic devices. Acc Chem Res 35(7):491–499

Nguyen NT, Ng KM, Huang X (2006) Manipulation of ferro fluid droplets using planar coils. Appl Phys Lett 89:052509

Niu X, Gulati S, Edel JB, deMello AJ (2008) Pillar-induced droplet merging in microfluidic circuits. Lab Chip 8(11):1837–1841

Ohashi T, Kuyama H, Hanafusa N, Togawa Y (2007) A simple device using magnetic transportation for droplet-based PCR. Biomed Microdevices 9(5):695–702

Paustian JS, Pascall AJ, Wilson NM, Squires TM (2014) Induced charge electroosmosis micropumps using arrays of Janus micropillars. Lab Chip 14(17):3300–3312

Pinheiro LB, Coleman VA, Hindson CM, Herrman J, Hindson BJ, Baht S, Emslie KR (2012) Evaluation of a droplet digital polymerase chain reaction format for DNA copy number quantification. Anal Chem 84(2):1003–1011

Protière S, Bazant MZ, Weitz DA, Stone HA (2010) Droplet breakup in flow past an obstacle: a capillary instability due to permeability variations. Europhys Lett 92(5):54002

Sayah A, Parashar VK, Pawlowski AG, Gijs MAM (2005) Elastomer mask for powder blasting microfabrication. Sens Actuators A 125(1):84–90

Sista RS, Eckhardt AE, Srinivasan V, Pollack MG, Palanki S, Pamula VK (2008) Heterogeneous immunoassays using magnetic beads on a digital microfluidic platform. Lab Chip 8(12):2188–2196

Song H, Bringer M, Tice J, Gerdts C, Ismagilov R (2003) Experimental test of scaling of mixing by chaotic advection in droplets moving through microfluidic channels. Appl Phys Lett 83(22):4664–4666

Song H, Chen DL, Ismagilov RF (2006) Reactions in droplets in microfluidic channels. Angew Chem Int Ed 45(44):7336–7356

Teh SY, Lin R, Hung LH, Lee AP (2008) Droplet microfluidics. Lab Chip 8(2):198–220

Teste B, Ali-Cherif A, Viovy JL, Malaquin L (2013) A low cost and high throughput magnetic bead-based immuno-agglutination assay in confined droplets. Lab Chip 13(12):2344–2349

Theberge AB, Courtois F, Schaerli Y, Fischlechner M, Abell C, Hollfelder F, Huck WTS (2010) Microdroplets in microfluidics: an evolving platform for discoveries in chemistry and biology. Angew Chem Int Ed 49(34):5846–5868

Van Reenen A, de Jong AM, den Toonder JMJ, Menno WJP (2014) Integrated lab-on-chip biosensing systems based on magnetic particle actuation—a comprehensive review. Lab Chip 14(12):1966–1986

Wang Y, Zhao Y, Cho SK (2007) Efficient in-droplet separation of magnetic particles for digital microfluidics. J Micromech Microeng 17(10):2148–2156

Zagnoni M, Cooper J (2009) On-chip electrocoalescence of microdroplets as a function of voltage, frequency and droplet size. Lab Chip 9(18):2652–2658